Egyptian Journal of Chemistry

http://ejchem.journals.ekb.eg/

A Successful Photodegradation of Organic Pollutant on the Surface of Novel Heterojunction Prepared by Sol-gel Method

Fouad A. F. Mohamed[a] , Mohamed A. Ahmed[a]*, Michel F. Abdel Messih[a], Maged S.Antonious[a]

[a] *Chemistry Department, Faculty of Science, Ain Shams University, El abbassia, Cairo 11566, Egypt*

Abstract

Herein, we report an innovative production of $BiVO_4$/ZnO nanocomposites with various compositions of $BiVO_4$ (0-20) wt % for successful alleviation of rhodamine B dye as cationic pollutant model. The promising direction for generation of ZnO nanoparticles was achieved by sol-gel route using triton-X-100 as templating agent. On the other hand, $BiVO_4$ nanoparticles were introduced on ZnO surface using chemical route. X-ray diffraction (XRD), energy dispersive spectroscopy (EDS), x-ray photoelectron spectroscopy (XPS), high resolution transmitted electron microscopy (HR-TEM), Brunauer-Emmett-Teller (BET) N_2-adsorption-desorption isotherms and diffuse reflectance spectroscopy (DRS) analysis were employed to elaborate the nanostructure, chemical compositions, oxidation state, pore structure and optical tendency of the solid specimens. The experimental results manifest the generation of bismuth vanadate with strong chemical affinity to ZnO surface. The incorporation of bismuth vanadate surface depresses the band gap energy of ZnO and controls the rate of recombination of the massive charge carriers. Anchoring 15 wt % of $BiVO_4$ on ZnO surface decomposes 90.8 % of RhB dye which attributes to the positive role of $BiVO_4$ in reducing the rate of charge carrier recombination. Positive holes and $OH^{\cdot}$ radicals are predominant species for the degradation process. The strikingly new nanocomposite is considered a promising photocatalyst for alleviation of organic pollutants from wastewater.

Keywords: bismuth vanadate /ZnO nanocomposite; sol-gel; semiconductor materials; photocatalyst; hydroxyl radicals;

1. Introduction

The disposal of toxic pollutants in wastewater affects the health of people and aquatic life. The traditional route for eliminating the organic pollutants such as adsorption, reverse osmosis, coagulation, flocculation and ion exchange are expensive and transport the primary pollutant into secondary one that must be treated at further processes [1-5]. The alleviation of organic pollutants from wastewater using solar energy technology is a promising route for limiting the environmental crisis [6-11]. To accomplish sustainable removal of toxic pollutants, it is critical to develop low cost and simple materials. Specifically, the process must be designed in a way that the production time and chemical use are minimized. ZnO is selected in our research due to the suitable band edges positions, good stability and nontoxicity [12-15]. Although ZnO still suffers from weak light absorption and high recombination rate of the massive charge carriers, yet the low cost of its metal precursors attracted various recent research [16-18]. One of the main factors of modification of ZnO is minimizing the recombination rate that occurs of the holes and electrons. So, for improving the photocatalytic behavior of ZnO, various species of metal ions were used as a dopant for ZnO to decrease the rate of recombination of photo-generated charge carriers. Particularly, the dopant ions that have a d^{10}

*Corresponding author e-mail: abdelhay71@hotmail@com.; (Mohamed A. Ahmed).
Received date 2023-05-03; revised date 2023-05-20; accepted date 2023-06-01
DOI: 10.21608/EJCHEM.2023.208771.7928
©2023 National Information and Documentation Center (NIDOC)

electronic configuration like: Bi^{3+}, In^{3+} and Ga^{3+} are considered highly promising cations for enhancing the ZnO performance [19-24]. Among these, doping of the photocatalyst using bismuth acquires great attention. Bismuth is a heavy metal so it could be considered a great alternative to noble metals. Bismuth is a cheap and environment-friendly material [25-30]. In addition, bismuth vanadate is considered an auspicious photocatalyst for hydrogen production and pollutant degradation. Bismuth vanadate is an n-type photoactive semiconductor with a band gap of 2.4 eV that can absorb a high range of visible light. The disadvantages of using the primitive bismuth vanadate as a photocatalyst arise from having a high electron-hole recombination rate with a low surface adsorption and weak charge transfer. However, when Bi^{3+} is incorporated into the crystal lattice of titanium dioxide (TiO_2), it improves its absorption edge and decreases the rate of recombination. Furthermore, incorporation of Bi^{3+} into the crystal lattice of ZnO is expected to increase the spectral range of ZnO and enhance the charge separation rate of electron-hole pairs of ZnO due to the difference in the sizes and electronic shell of zinc and bismuth ions.

Herein, various proportions of $BiVO_4$ are incorporated on ZnO surface in attempt to decompose rhodamine B dye under UV irradiations. The as-synthesized samples are fully characterized by developed techniques as x-ray diffraction (XRD), x-ray photoelectron spectroscopy (XPS), Brunauer-Emmett-Teller (BET) analysis, diffuse reflectance spectroscopy (DRS), photoluminescence spectroscopy (PL), transmitted electron microscopy (TEM) and energy dispersive spectroscopy (EDS).

2. Materials and characterization

2.1. chemicals

All chemicals were of pure grade (B.D.H and Merck) and were used without further purification. Zinc acetate dihydrate, ammonium hydroxide, triton-X-100, bismuth nitrate pentahydrate, terephthalic acid and ammonium metavanadate were purchased from Merck. Ethylene glycol anhydrous and rhodamine B dye were purchased from B.D.H.

2.2. Preparation of the photocatalyst

2.2.1. Formulation of Zinc oxide nanoparticles

ZnO nanoparticles were prepared using sol-gel method [14]. Firstly, a definite concentration of Triton-X-100 solution was introduced gradually and with a constant stirring for 3 hours to a solution of $Zn(CH_3COO)_2$. After that, ammonium hydroxide (1molar) was added to the previous stirring vigorously till the pH of the produced sol is equal 8, then the produced sol was exposed to constant stirring for 3 hours. To control the formulation of the produced gel nanoparticles, the sol was left for 2 days. Finally, the produced gel was filtered and dried at 80°C for 10 hours. Then, the sample calcinated at 400 °C for 3 hours in a furnace muffle.

2.2.2. Formulation of bismuth vanadate and (bismuth vanadate / zinc oxide) nanoparticles

The studied composite samples are denoted as ZnBi5, ZnBi10, ZnBi15 and ZnBi20 corresponding to samples of zinc oxide nanoparticles containing 5, 10, 15 and 20 wt % of bismuth vanadate, respectively.

Bismuth vanadate nanoparticles were prepared by mixing bismuth nitrate with 1 ml ethylene glycol followed by stirring for 1 hour then adding dropwise an appropriate amount of ammonium metavanadate. The mixture was then stirred for 3 hours. The resulting suspension solution was then filtered, washed with deionized water several times to eliminate any impurities then dried at 100°C for 5 hours.

The composite samples were prepared by the same procedure of preparing bismuth vanadate stated above with introducing appropriate amounts of zinc oxide and stirring vigorously for 2 hours before adding ammonium metavanadate mixture in the above-mentioned procedure.

2.3. Material characterization

X-ray diffraction (XRD) (P-Analytical X'PERT MPD diffractometer) with copper anode emitting Kα radiation was used for examining the diffraction patterns of the produced samples with an angle from 10 º to 70 º. To investigate the porosity and the surface properties of the samples, the adsorption-desorption isotherms of nitrogen were examined for the samples at 77 K. For analyzing the size and the nanostructures of the produced samples, a high-resolution transmission electron microscope

(HRTEM, JEM2100, Jeol, Japan) device was used for examination of selected samples. Energy dispersive x-ray spectroscopy (EDS, Quanta FEG - 250) was used for investigation of the elements on the solid surface of the sample. The x-ray photoelectron spectroscopy (XPS) analysis was proceeded using K-ALPHA (Thermo Fisher Scientific, USA) instrument with monochromatic x-ray Al Kα radiation from 10 to 1350 eV. Diffuse reflectance spectroscopy (DRS) and optical measurements were measured using uv-vis spectrophotometer (V-770 Jasco spectrophotometer). The DRS results are recorded as reflectance (%) against wavelength [F(R)=(1-R^2/2R)] where R is the reflectance. For analyzing the hydroxyl radical formation, a lumina fluorescence spectrophotometer (Thermo fisher Scientific) was used. A COD device (MRC labs, DBR-001N) is used for measuring the chemical oxygen demand (COD) for a selected sample.

2.4. Photocatalytic degradation of rhodamine B dye

As a model of organic pollutant, rhodamine B dye was chosen to evaluate the photocatalytic performances of the prepared samples under investigation using 16-watt Hg lamp at 365 nm wavelength. The samples were tested under dark conditions for one hour and under illumination conditions for 6 hours. The dye concentration was $1.5x10^{-5}$ mole/liter. A 0.1 g from each sample was mixed with 100 ml of rhodamine B dye under uv illumination for 6 hours.

3. Results and discussion

3.1. X-ray diffraction (XRD)

The crystallinity of ZnO and the prepared nanocomposites were investigated through XRD and are depicted in Fig.1. The characteristic peaks at 2θ = 31.80, 34.41, 36.24, 47.58, 56.64, 62.94, 66.30, 67.98, and 69.15 that correspond to (100),(002),(101),(102),(110),(103),(200),(112) and(201) planes characterize ZnO nanoparticles [18,31] and referred to the presence of the wurtzite structure corresponding to the card number (JCPDS 36-1451). After modifying the ZnO by various amounts of $BiVO_4$, different diffraction peaks have appeared which indicate the incorporation of $BiVO_4$ into the lattice of ZnO nanostructure. The crystallite size of the prepared samples calculated by the Debye–Scherrer equation were 30, 25, 31, 55 and 31.7 nm for ZnO, ZnBi5, ZnBi10, ZnBi15 and ZnBi20, respectively. It is also noted that some diffraction peaks of zinc vanadate appeared as a result of the interaction between the primitive zinc oxide nanoparticles and ammonium vanadate during the composite preparation process.

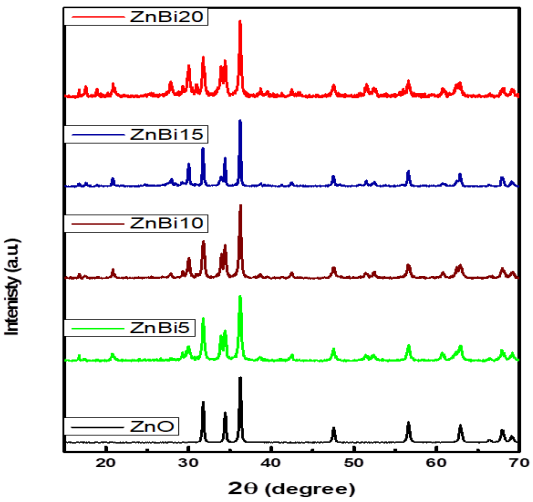

Fig. 1: X-ray diffraction pattern of ZnO, ZnBi5, ZnBi10, ZnBi15 and ZnBi20.

3.2. Surface characterization

Fig. 2 represents N_2 adsorption-desorption isotherms for ZnBi5, ZnBi10, ZnBi15, and ZnBi20 nanoparticles at 77 K. According to IUPAC classifications of the adsorption isotherms, all produced charts are obeying type II isotherms with H3 hysteresis loop which refer to slit-shape structure of the pores. The surface area of ZnBi5, ZnBi10, ZnBi15 and ZnBi20 calculated using BET equation are 14.58, 14.52, 12.43 and 7.84 m^2/g. The formulation of $BiVO_4$ /ZnO nanocomposites caused a little reduction of the surface area of ZnO in all samples which are accompanied by the remarkable shrinking in the hysteresis loop.

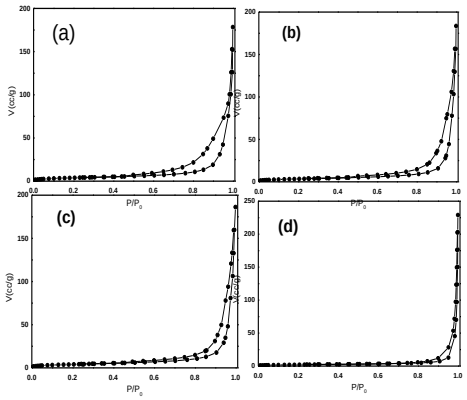

Fig. 2: N_2-adsorption-desorption isotherm for (a)ZnBi5, (b)ZnBi10, (c) ZnBi15 and (d)ZnBi20.

Fig. 3 illustrates HR-TEM images of the primitive ZnO, $BiVO_4$ and a prepared nanocomposite sample (ZnBi15). As shown in Fig.3 a, ZnO is observed having cubic crystalline shape with 28 nm average particle size (which is in good agreement with value of 30 nm obtained using XRD), while $BiVO_4$ in Fig.3 b appears as sheet structure. The strong attachment of cubic ZnO nanoparticles to $BiVO_4$ sheets is clearly observed as depicted in Fig.3 c.

Fig. 4 represents the EDS mapping for ZnBi15 sample that shows the presence and a well distribution of Zn, Bi, V and O among the ZnBi15 sample. So, the suggestion of uniform distribution of $BiVO_4$ on the surface of ZnO can be confirmed.

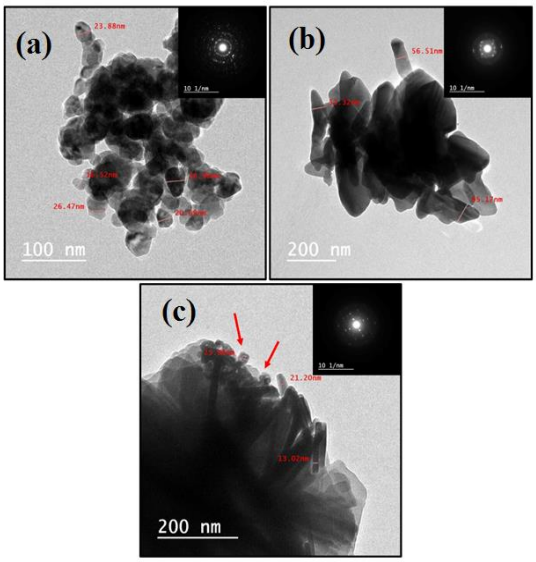

Fig. 3: High-resolution transmission electron microscopy images of (a)ZnO (b)Bismuth vanedate and (c)ZnBi15.

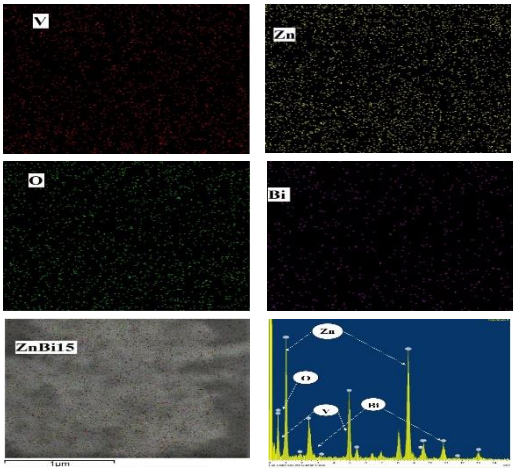

Fig. 4: Energy-dispersive x-ray spectroscopy and mapping of ZnBi15.

3.3. X-ray photoelectron spectroscopy (XPS)

The XPS spectrogram of ZnBi15 sample is represented in Fig. 5. The figure indicates that the Zn, O, V and Bi elements are presented in the examined sample. There are two characteristic peaks for ZnO nanoparticles that appear at 1021.1 eV and 1044.3 eV corresponding to the binding energy of zinc at $2p_{3/2}$ and $2p_{1/2}$, respectively [31]. The peaks at 533.3 eV, 531.9 eV and 530.6 eV are referring to the different forms of oxygen in the nanocomposite structure: adsorbed oxygen on the surface, oxygen vacancy and the oxygen in the lattice sample [32]. The two peaks detected at 523.8 eV and 516.4 eV in the spectra of V 2p are attributed to V $2p_{1/2}$ and V $2p_{3/2}$, respectively. These two peaks are characteristic to V^{5+} ion that is present in the crystal lattice of $BiVO_4$[33]. The doublet peaks existed at 158.5 eV and 163.9 eV are referred to Bi $4f_{7/2}$ and Bi $4f_{5/2}$, respectively [33]. Presence of the two characteristic peaks of Bi^{3+} and V^{5+} cation confirm the formation of bismuth vanadate species in the composite.

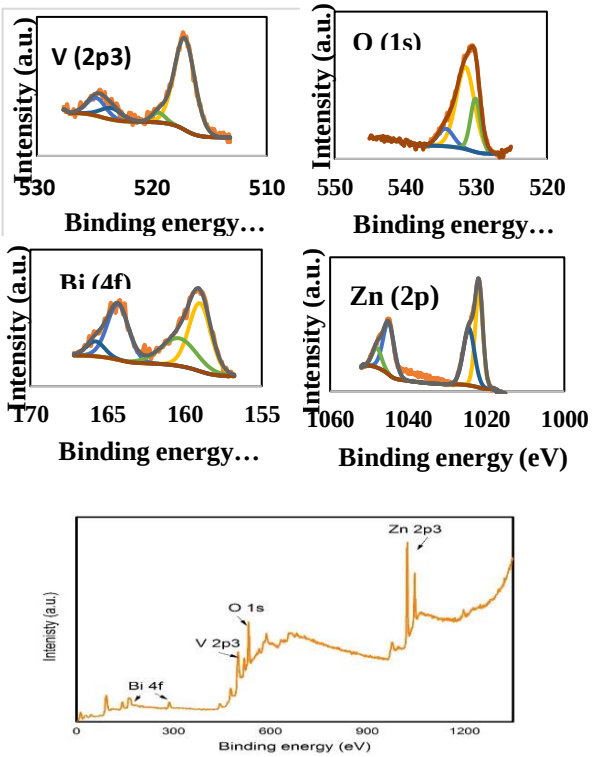

Fig. 5: X- ray photoelectron spectroscopy spectra of Bi(4f) , V(2p), O(1s) and Zn(2p) of ZnBi15.

3.4. Optical properties

The DRS analysis is employed for determination of the absorption performance of the formulated photocatalyst. Fig. 6 represents the DRS analysis and Tauc plot for primitive nanoparticles and $BiVO_4$/ZnO heterojunction. The DRS analysis shows presence of a strong absorption band edge around 397 nm for ZnO which is attributed to the electron excitation between valence band and conduction band, the absorption band edge for $BiVO_4$ appears at 575 nm in the visible region. As represented in Fig. 6 c, the absorption ability of ZnBi15 sample is significantly improved compared to that of primitive ZnO. The absorption edge of ZnBi15 sample is located at 416 nm which increases the ability of the nanocomposite to absorb in the visible region.

According to Kubelka Munk formula [34], the band gap energy (E_g) can be estimated by constructing Tauc diagram. This method assumes that the energy-dependent absorption coefficient "α" can be expressed by the equation.

$$(\alpha h\upsilon)^{1/n} = A\,(h\upsilon - E_g)$$

where $h\upsilon$ is the incident energy of photon, E_g is the energy bandgap and" A" is a constant value. The value of" n" is equal to 0.5 or 2 for the direct and indirect electronic transitions [34].

Fig. 6 d,e,f shows the tauc plot for primitive nanoparticles and bismuth vanadate/zinc oxide heterojunction. The extrapolation of the linear region estimates the energy difference between V_b and C_b (Eg). The estimated values of direct Eg of the samples are 3.13, 2.16 and 2.98 for the pure ZnO, $BiVO_4$, and ZnBi15, respectively.

At the point of zero charge of semiconductor, the valence and conduction band edges can be estimated using these equations [35]:

$$E_{VB} = X - E_e + 0.5E_g$$
$$E_{CB} = E_{VB} - E_g$$

where E_{Vb} and E_{CB} represent the valence and conduction band edges of the semiconductor, respectively; E_e is the value of free electron energy on the scale of hydrogen and its value is 4.5 eV and X is the geometrical mean of electronegativity of the semiconductor calculated from the absolute values of electronegativity of the constituent semiconductor atoms [35]. The value of [X] is calculated to be 5.79 for the primitive ZnO and 6.04 for $BiVO_4$ [35,36]. By calculating the E_{VB} and E_{CB} of ZnO and $BiVO_4$ using the above equations, the mechanism of electron transfer between ZnO and $BiVO_4$ could be predicted. ZnO displays conduction band energy (E_{CB}= - 0.27 eV) and valence band energy (E_{VB}=+2.86 eV) whereas, $BiVO_4$ has (E_{CB}= +0.46 eV) and (E_{VB}= +2.62 eV). According to the values of E_{CB} and E_{VB} of the two semiconductors, electrons leap over freely from the conduction band of ZnO to the conduction band of $BiVO_4$ which is less negative across the interfacial surface between the two materials. In addition, the positive holes migrate from the valence band of ZnO to that of $BiVO_4$. This mechanism of charge transfer of the charge carriers decreases the rate of recombination by increasing the lifetime of the electrons and holes and augments the quantum efficiency of the photogenerated charges.

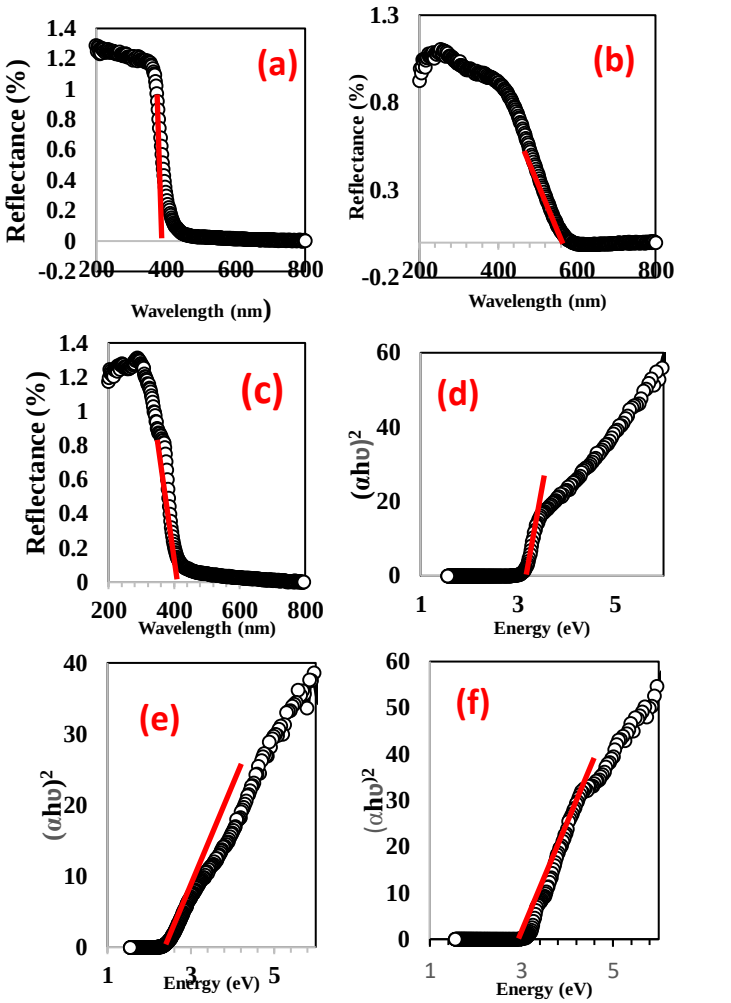

Fig. 6: Diffuse reflectance spectroscopy plots of (a)ZnO, (b)$BiVO_4$ and (c) ZnBi15 and Tauc plots of (d)ZnO, (e)$BiVO_4$ and (f) ZnBi15.

3.5. Photocataytic performance

For comparing the effectiveness of the prepared photocatalysts, photocatalytic performances of all the studied samples were tested using rhodamine B dye under uv light. The results obtained for the percentages of removal of dye using uv illumination are 27.4, 46.0, 62.7, 72.0, 90.8 and 28.5 % for $BiVO_4$, ZnO, ZnBi5, ZnBi10, ZnBi15 and ZnBi20, respectively.

Fig. 7 summarizes the reaction kinetics of rhodamine B degradation under light irradiation over the primitive samples of $BiVO_4$, ZnO and the prepared nanocomposites ZnBi5, ZnBi10, ZnBi15 and ZnBi20 samples. The pseudo first order rate constants estimated are found to be $0.7x10^{-3}$, $1.5x10^{-3}$, $2.3x10^{-3}$, $3.2x10^{-3}$, $6.4x10^{-3}$ and $0.5x10^{-3}$ over for $BiVO_4$, ZnO, ZnBi5, ZnBi10, ZnBi15 and ZnBi20, respectively. The figure clarifies that increasing the dopant composition augments the photochemical degradation performance up to a certain percentage of dopant followed by observable decreasing of the efficiency at higher amounts.

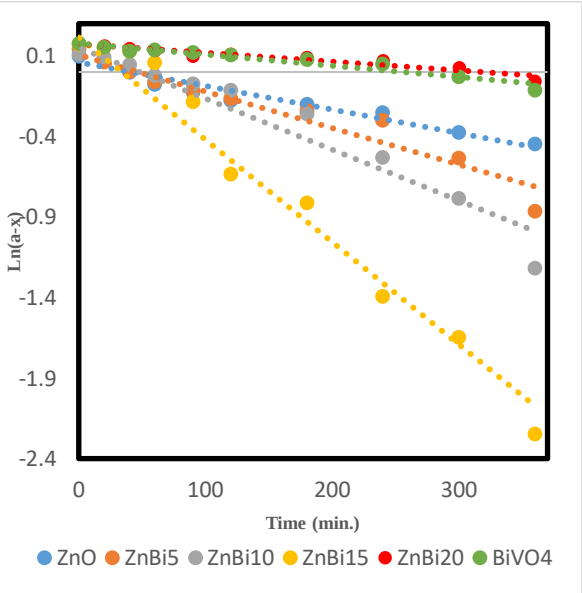

Fig. 7: Kinetics of degradation of rhodamine B dye over bismuth vanadate, ZnO, ZnBi5, ZnBi10, ZnBi15 and ZnBi20 with ZnBi15 showing highest degradation performance.

The 2-hydroxy terephthalic acid has a photoluminescence maximum wavelength peak at 423nm as depicted in fig. 8(a-c). It is to be noted that increasing of the peak intensity with increasing the illumination time is considered an important indication about the production of high quantity of $OH^{\cdot}$ radicals under illumination [37]. The amount of hydroxyl radicals that are generated in presence of $BiVO_4$ (Fig.8b) are very low. In contrary, after using $BiVO_4$ to enhance the photocatalytic performance of ZnO, the rate of generation of hydroxyl radical of ZnO catalyst is increased (Fig. 8c).

The types of produced active radicals and oxygen species during the photodegradation process of RhB dye over ZnBi15 are examined by proceeding the photochemical degradation process in presence of several scavengers such as silver nitrate, ammonium oxalates, isopropanol and benzoquinone to identify the role of various active species in the degradation process [38]. Fig. 9a depicts the effect of using of different scavengers in the degradation process. As represented in fig. 9a, using silver nitrate as scavenger for trapping the conduction band electrons did not make a big change in the degradation percentage. This role off the mechanism of electron reduction to participate in the photocatalytic degradation process. Conversely, the photodegradation process is notably decreased by using benzoquinone and isopropanol. This means that the major reactive species for the degradation process are the superoxide radical anion ($O_2^{\cdot-}$) and hydroxyl radicals. In addition, using ammonium oxalate as scavenger mildly affects the rate of degradation indicating that the positive hole (h^+) has less role in the degradation process.

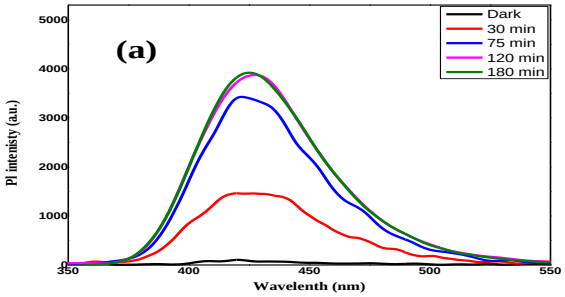

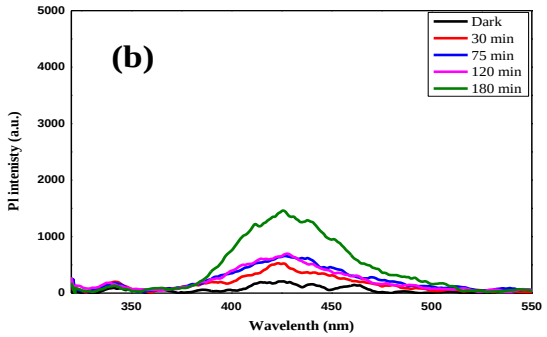

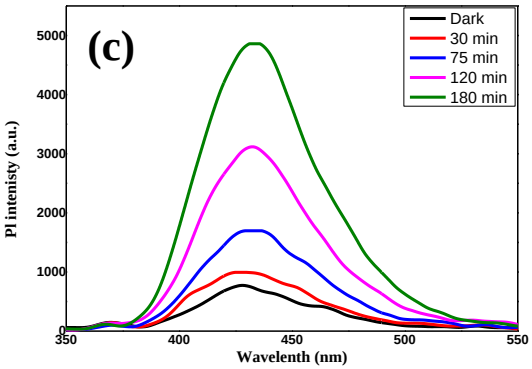

Fig. 8: Photoluminescence of 2-hydroxy terephthalic acid over the surface of (a)zinc oxide, (b) Bismuth vanadate and (c)ZnBi15.

For examining the stability of $BiVO_4$/ZnO nanocomposites, ZnBi15 was subjected to a number of consecutive photocatalytic cycles under light irradiation as depicted in Fig.9b. The figure indicates that the photocatalyst keeps 70% of its activity after the fifth cycle. Thus, the photocorrosion of Bi^{3+} is inhibited to a considerable extent.

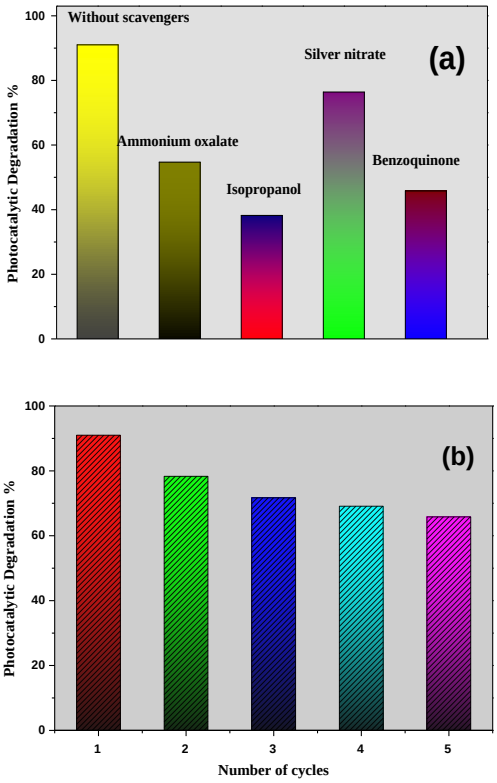

Fig.9: (a) the photocatalytic degradation of ZnBi15 sample using different scavengers, (b) five consecutive photocatalytic cycles for degradation of rhodamine B using ZnBi15.

The effect of changing the pH of the degradation medium is fulfilled. The photocatalytic degradation process is performed at different pH's (3,5,7,9). As represented in Fig.10, it is clear that the suitable medium for the degradation process is at pH= 7. By varying the pH to strongly acidic or basic medium, a remarkably decrease in the degradation rate is noted. This may be ascribed to the dissolution of the ZnO in the relatively acidic and basic mediums.

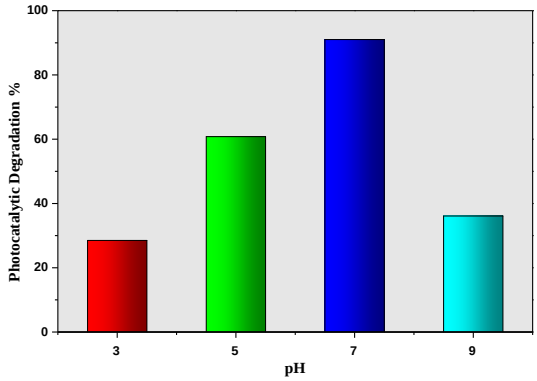

Fig10: The degradation percentage of ZnBi15 sample at different pH degradation bath.

In order to evaluate whether the action of the prepared catalyst is degradation or decolorization of the dye, the COD analysis is performed for the dye before and after the degradation process. It has been found that the COD value is 59 ppm for RhB of concentration $1.5x10^{-5}$ mole/liter while after 6 hours of degradation using 0.1 g of ZnBi15 sample under near uv illumination the COD value shrunk to 9 ppm. This measurable decreasing in the COD value indicates that the decreasing in the absorbance of the dye samples by time is a degradation not decolorization of the dye.

4. Conclusion

$BiVO_4$/ZnO heterojunction is constructed through two steps chemical route for decomposition of rhodamine B dye. Heterojunction with 15 wt% $BiVO_4$ is the optimum sample that decomposes more than 90% of RhB dye. The samples are characterized by different techniques including X-ray diffraction (XRD), energy dispersive spectroscopy (EDS), x-ray photoelectron spectroscopy (XPS), high resolution transmitted electron microscopy (HR-TEM), Brunauer-Emmett-Teller (BET) N_2-adsorption-desorption isotherms and diffuse reflectance spectroscopy (DRS) analysis. The

effect of scavengers shows that hydroxyl and superoxide radicals are the most reactive species in the photodegradation of RhB. In addition, photocatalytic reaction of rhodamine B over the prepared samples is kinetically pseudo first order reaction. The chemical oxygen demand (COD) is assayed and it indicates that rhodamine B dye is chemically depredated not only its color removed.

5. Conflicts of interest

There is no conflict of interest to report.

6. References

[1] Y.Zhang, Yi.Xiao,G.Xu, D.Wang, J.Li, J.Huang, Z.Jin; **Preparation of Fe_2O_3 porous microspheres modified pumice and its adsorption performance on phosphate removal**, Journal of Environmental Chemical Engineering,11(2023)109995.

[2] A.Skotta, A.Jmiai, W.Elhayaoui, A.El-Asri, M.Tamimi, A.Assabbane, S.El Issami; **Suspended matter and heavy metals (Cu and Zn) removal from water by coagulation/flocculation process using a new Bio-flocculant: Lepidium sativum**, Journal of the Taiwan Institute of Chemical Engineers, 145(2023)104792.

[3] M. Adel, M.A. Ahmed , A.A. Mohamed; **Synthesis and characterization of magnetically separable and recyclable crumbled $MgFe_2O_4$/reduced graphene oxide nanoparticles for removal of methylene blue dye from aqueous solutions**, J. Phys. Chem. Solid 149 (2021)109760.

[4] M. Adel, M. A. Ahmed, A. A. Mohamed; **A facile and rapid removal of cationic dyes using hierarchically porous reduced graphene oxide decorated with manganese ferrite,** Flat Chem., 26 (2021)100233.

[5] H.Pezeshki, M.Hashemi, S.Rajabi**; Removal of arsenic as a potentially toxic element from drinking water by filtration: A mini review of nanofiltration and reverse osmosis techniques**, Heliyon, 9(2023)e14246.

[6] M.A. Ahmed, A. Fahmy, M.G. Abo-Zaed; E.M. Hashem; **Fabrication of novel $AgIO_4/SnO_2$ heterojunction for photocatalytic hydrogen production through direct Z-scheme mechanism,** J. Photochem. Photobiol., 400(2020)112660.

[7] T.H.Pham, M.H.Tran, T.T. Chu, Y.Myung, S.H. Jung, M.G.Mapari, K.Taeyoung; **Enhanced photodegradation of tetracycline in wastewater and conversion of CO_2 by solar light assisted ZnO/g-C_3N_4**, Environmental Research, 217(2023)114825.

[8] Ali Alsalme, A.H. Galal, E. F. El-Sherbeny, A. Soltan, M.F. Abdel-Messih, M.A. Ahmed; **Fabrication of S-scheme TiO_2/g-C_3N_4 nanocomposites for generation hydrogen gas and removal of fluorescein dye,** Diamond Related Maters., 122 (2022) 108819.

[9] M. Beneissa, N. Abbas, S. Al Arni, N. Elboughdiri, A. Moumen, M. S. Hamdy, H. S.M. Abd-Rabboh, A.H. Galal, M. Gad Al-Metwaly, M.A. Ahmed; **$BiVO_3$/g-C_3N_4 S-scheme heterojunction nanocomposite photocatalyst for hydrogen production and amaranth dye removal;** Optical Mater. ,118 (2021) 111237.

[10] O.Mertah, A.Gomez-Aviles, A.Kherbeche, C.Belver, J.Bedia; **Peroxymonosulfate enhanced photodegradation of sulfamethoxazole with TiO_2@$CuCo_2O_4$ catalysts under simulated solar light**, Journal of Environmental Chemical Engineering, 10(2022)108438.

[11] H.S.M. Abd-Rabboh, A.H. Galal, R. Abdel Aziz, M. A. Ahmed, **novel $BiVO_3/SnO_2$ step S-scheme nano heterojunction for an enhanced visible light photocatalytic degradation of amaranth dye and hydrogen production**; Royal Soc. Chem. Adv. , 11 (2021) 29507.

[12] M.A. Ahmed, Z.M. Abou-Gamra, M.A. ALshakhanbeh, H. Medien; **Control synthesis of metallic gold nanoparticles homogeneously distributed on hexagonal ZnO nanoparticles for photocatalytic degradation of methylene blue dye;** Environ. Nanotechnol. Monitor. Manag., 12 (2019) 100217.

[13] L.H.Mohammed, F.Gulbagca, R.N.Tiri, A.Aygun, M.Bekmezci, F.Sen, **Hydrothermal-assisted synthesis of Co-doped ZnO nanoparticles catalyst for sodium borohydride dehydrogenation and photodegradation of organic pollutants in water**, Chemical Engineering Journal Advances, 14(2023)100495.

[14] M.F. Abdel Messih, M.A. Ahmed, A. Soltan, S. S. Anis; **Synthesis and characterization of novel Ag/ZnO nanoparticles for photocatalytic degradation of methylene blue under UV and solar irradiation;** J. Phys. Chem. Solids, 135 (2019) 109086.

[15] M. S. Hamdy, H.S.M. Abd-Rabboh, M. Beneissa, M. G. Al-Metwaly, A.H. Glal; M.A. Ahmed; **Fabrication of novel polyaniline/ZnO heterojunction for exceptional photocatalytic hydrogen production and degradation of fluorescein dye through direct Z-scheme mechanism,** Optical Maters. 117 (2021) 111198.

[16] E.M. Ezz el-regal, M.A. Ahmed,_M.F. Abdel-Messih, Z.M. Abou-Gamra; **Synthesis of novel ZnO nanoparticles with exceptional crystalline and photocatalytic features toward recalcitrant pollutant: Fluorescein dye**, Optical Maters., 111 (2021) 110597.

[17] C. Gomez-Solis, J.C. Ballesteros, L.M. Torres-Martínez , I. Juárez-Ramírez, L.A. Díaz Torres , M. E. Zarazua-Morin, S. W. Lee; **Rapid synthesis of ZnO nano-corncobs from Nital solution and its application in the photodegradation of methyl orange** , Journal of Photochemistry and Photobiology A: Chemistry, 298 (2014) 49.

[18] M. F. Abdel Messih, A.E. Shalan, M.F Sanad, M. A. Ahmed; **Facile approach to prepare ZnO@SiO_2 nanomaterials for photocatalytic degradation of some organic pollutant models,** J. Maters. Sci. Materials in Electronics, 30 (2019) 1491.

[19] K.S.Khashan, M.Mahdi ; **Preparation of indium-doped zinc oxide nanoparticles by pulsed laser ablation in liquid technique and their characterization**. Appl Nanosci., 7(2017) 589.

[20] S.Pati,P.Banerji,S.B.Majumder ;**Properties of indium doped nanocrystalline ZnO thin films and their enhanced gas sensing performance**, **RSC Adv.,** 5(2015) 61230.

[21] H. Gomez , A. Maldonado , M. de la L. Olvera,D.R.Acosta; **Gallium-doped ZnO thin films deposited by chemical spray ,** Solar Energy Materials and Solar Cells, 87(2005) 107.

[22] K.Kim, J.Moon; **Three-Dimensional Bicontinuous $BiVO_4$/ZnO Photoanodes for High Solar Water-Splitting Performance at Low Bias Potenti**al, ACS Appl. Mater. Interfaces, 10(2018) 34238.

[23] K. Wannakan, K. Khansamrit, T.Senasu, S.Nanan**; Ultrasound-Assisted Synthesis of a ZnO/$BiVO_4$ S-Scheme Heterojunction Photocatalyst for Degradation of the Reactive Red 141 Dye and Oxytetracycline Antibiotic** ,ACS Omega, 8 (2023) 4835.

[24] M.Alhaddad a, M.Amin, Z.Zaki; **Novel $BiVO_4$/ZnO heterojunction for amended photoreduction of mercury (II) ions**, Optical Materials,127(2022)112251

[25] M.F.R. Samsudin, S. Sufian, R. Bashiri, N.M. Mohamed , L.T. Siang , R.M. Ramli; **Optimization of photodegradation of methylene blue over modified TiO_2/$BiVO_4$ photocatalysts: effects of total TiO_2 loading and different type of co-catalyst,** Maters Today: Proceedings, 5(2018)21710.

[26] C. Ma, M. Wei; **$BiVO_4$-nanorod-decorated rutile/anatase TiO_2 nanofibers with enhanced photoelectrochemical performance**, Matters. Lett., 125(2020)126849.

[27] Y.R. Lv, C.J. Liu, R.K. He, X. Li, Y.H. Xu, **$BiVO_4$/TiO_2 heterojunction with enhanced photocatalytic activities and photoelectochemistry performances under visible light illumination;** Matters. Res. Bullet., 117(2019) 35.

[28] Y. Hu, D. Li, Y. Zheng, W. Chen, G. Xiao; **$BiVO_4$/TiO_2 nanocrystalline heterostructure: A wide spectrum responsive photocatalyst towards the highly efficient decomposition of gaseous benzene,** Appl. Catal. B., 27(2011) 30.

[29] Z. Guo, P. Li, H. Che, G. Wang, J. Mu**; One-dimensional spindle-like BiVO4/TiO_2 nanofibers heterojunction nanocomposites with enhanced**

visible light photocatalytic activity, Ceramic Int., 42(2016)4517.

[30] Q. Li, W. Zhao, Z. Zhai, K. Ren, T. Wang, H. Guan, H. Shi; **2D/2D Bi_2MoO_6/g-C_3N_4 S-scheme heterojunction photocatalyst with enhanced visible-light activity by Au loading,** J. Maters. Sci. Technol., 56(2020)216.

[31] S.S. Patil, M.G. Mali, M.S. Tamboli, D.R. Patil, M.V.Kulkarni, H.Yoon, H.Kim, S.S.Al-Deyab, S.S.Yoon, S.S.Kolekar,B.B.Kale;**Green approach for hierarchical nanostructured Ag-ZnO and their photocatalytic performance under sunlight**,Catalysis Today, 260(2016)126.

[32] J.Zhou , Y.Zhang, S.Li , J.Chen ; **Ni/NiO Nanocomposites with Rich Oxygen Vacancies as High-Performance Catalysts for Nitrophenol Hydrogenation**, *Catalysts*, 11(2019)944.

[33] K.Hemavibool, T.Sansenya, S.Nanan; **Enhanced Photocatalytic Degradation of Tetracycline and Oxytetracycline Antibiotics by $BiVO_4$ Photocatalyst under Visible Light and Solar Light Irradiation**, Antibiotics, 11(2022)761.

[34]B.Xiao, L.Lin, J.Hong,H.Lin,Y.Song; **Synthesis of a monoclinic BiVO4 nanorod array as the photocatalyst for efficient photoelectrochemical water oxidation**, RSC Adv. , 7(2017)7547.

[35] Y.Chen, X.Ma, D.Li, H.Wang, C.Huang'**Mechanism of enhancing visible-light photocatalytic activity of $BiVO_4$ via hybridization of graphene based on a first-principles study**,RSC Adv. , 7(2017) 4395.

[36] F. Uz Zaman, B. Xie, J. Zhang, T.Gong, K. Cui, L. Hou, J. Xu, Z.Zhai,C.Yuan; **MOFs Derived Hetero-ZnO/Fe_2O_3 Nanoflowers with Enhanced Photocatalytic Performance towards Efficient Degradation of Organic Dyes**, Nanomaterials , 11(2021)3239.

[37] G.Zerjav, A.Albreht, I.Vovk, A.Pintar**; Revisiting terephthalic acid and coumarin as probes for photoluminescent determination of hydroxyl radical formation rate in heterogeneous photocatalysis**, App. Cat. A: general , 25(2020)117566.

[38]A.Alsulmi, M.Shaker, A.Basely, M. Abdel-Messih, A.Sultan , M.Ahmed; **Engineering S-scheme Ag_2CO_3/g-C_3N_4 heterojunctions sonochemically to eradicate Rhodamine B dye under solar irradiation**, RSC Advances, 13(2023) 12229.